

Measurement of the differential $\gamma + c$ -jet cross section and the ratio of differential $\gamma + c$ and $\gamma + b$ cross sections in $p\bar{p}$ collisions at $\sqrt{s} = 1.96$ TeV

V.M. Abazov,³² B. Abbott,⁶⁹ B.S. Acharya,²⁶ M. Adams,⁴⁷ T. Adams,⁴⁵ G.D. Alexeev,³² G. Alkhazov,³⁶
A. Alton^{a,58} A. Askew,⁴⁵ S. Atkins,⁵⁶ K. Augsten,⁷ C. Avila,⁵ F. Badaud,¹⁰ L. Bagby,⁴⁶ B. Baldin,⁴⁶
D.V. Bandurin,⁴⁵ S. Banerjee,²⁶ E. Barberis,⁵⁷ P. Baringer,⁵⁴ J.F. Bartlett,⁴⁶ N. Bartosik,³⁹ U. Bassler,¹⁵
V. Bazterra,⁴⁷ A. Bean,⁵⁴ M. Begalli,² L. Bellantoni,⁴⁶ S.B. Beri,²⁴ G. Bernardi,¹⁴ R. Bernhard,¹⁹ I. Bertram,⁴⁰
M. Besançon,¹⁵ R. Beuselinck,⁴¹ P.C. Bhat,⁴⁶ S. Bhatia,⁶⁰ V. Bhatnagar,²⁴ G. Blazey,⁴⁸ S. Blessing,⁴⁵ K. Bloom,⁶¹
A. Boehnlein,⁴⁶ D. Boline,⁶⁶ E.E. Boos,³⁴ G. Borissov,⁴⁰ A. Brandt,⁷² O. Brandt,²⁰ R. Brock,⁵⁹ A. Bross,⁴⁶
D. Brown,¹⁴ J. Brown,¹⁴ X.B. Bu,⁴⁶ M. Buehler,⁴⁶ V. Buescher,²¹ V. Bunichev,³⁴ S. Burdin^{b,40} C.P. Buszello,³⁸
E. Camacho-Pérez,²⁹ B.C.K. Casey,⁴⁶ H. Castilla-Valdez,²⁹ S. Caughron,⁵⁹ S. Chakrabarti,⁶⁶ D. Chakraborty,⁴⁸
K.M. Chan,⁵² A. Chandra,⁷⁴ E. Chapon,¹⁵ G. Chen,⁵⁴ S. Chevalier-Théry,¹⁵ S.W. Cho,²⁸ S. Choi,²⁸
B. Choudhary,²⁵ S. Cihangir,⁴⁶ D. Claes,⁶¹ J. Clutter,⁵⁴ M. Cooke,⁴⁶ W.E. Cooper,⁴⁶ M. Corcoran,⁷⁴ F. Couderc,¹⁵
M.-C. Cousinou,¹² A. Croc,¹⁵ D. Cutts,⁷¹ A. Das,⁴³ G. Davies,⁴¹ S.J. de Jong,^{30,31} E. De La Cruz-Burelo,²⁹
F. Déliot,¹⁵ R. Demina,⁶⁵ D. Denisov,⁴⁶ S.P. Denisov,³⁵ S. Desai,⁴⁶ C. Deterre,¹⁵ K. DeVaughan,⁶¹ H.T. Diehl,⁴⁶
M. Diesburg,⁴⁶ P.F. Ding,⁴² A. Dominguez,⁶¹ A. Dubey,²⁵ L.V. Dudko,³⁴ D. Duggan,⁶² A. Duperrin,¹² S. Dutt,²⁴
A. Dyshkant,⁴⁸ M. Eads,⁶¹ D. Edmunds,⁵⁹ J. Ellison,⁴⁴ V.D. Elvira,⁴⁶ Y. Enari,¹⁴ H. Evans,⁵⁰ A. Evdokimov,⁶⁷
V.N. Evdokimov,³⁵ G. Facini,⁵⁷ L. Feng,⁴⁸ T. Ferbel,⁶⁵ F. Fiedler,²¹ F. Filthaut,^{30,31} W. Fisher,⁵⁹ H.E. Fisk,⁴⁶
M. Fortner,⁴⁸ H. Fox,⁴⁰ S. Fuess,⁴⁶ A. Garcia-Bellido,⁶⁵ J.A. García-González,²⁹ G.A. García-Guerra^{c,29}
V. Gavrilov,³³ P. Gay,¹⁰ W. Geng,^{12,59} D. Gerbaudo,⁶³ C.E. Gerber,⁴⁷ Y. Gershtein,⁶² G. Ginther,^{46,65}
G. Golovanov,³² A. Goussiou,⁷⁶ P.D. Grannis,⁶⁶ S. Greder,¹⁶ H. Greenlee,⁴⁶ G. Grenier,¹⁷ Ph. Gris,¹⁰ J.-F. Grivaz,¹³
A. Grohsjean^{d,15} S. Grünendahl,⁴⁶ M.W. Grünewald,²⁷ T. Guillemin,¹³ G. Gutierrez,⁴⁶ P. Gutierrez,⁶⁹ J. Haley,⁵⁷
L. Han,⁴ K. Harder,⁴² A. Harel,⁶⁵ J.M. Hauptman,⁵³ J. Hays,⁴¹ T. Head,⁴² T. Hebbeker,¹⁸ D. Hedin,⁴⁸
H. Hegab,⁷⁰ A.P. Heinson,⁴⁴ U. Heintz,⁷¹ C. Hensel,²⁰ I. Heredia-De La Cruz,²⁹ K. Herner,⁵⁸ G. Hesketh^{f,42}
M.D. Hildreth,⁵² R. Hirosky,⁷⁵ T. Hoang,⁴⁵ J.D. Hobbs,⁶⁶ B. Hoeneisen,⁹ J. Hogan,⁷⁴ M. Hohlfeld,²¹
I. Howley,⁷² Z. Hubacek,^{7,15} V. Hynek,⁷ I. Iashvili,⁶⁴ Y. Ilchenko,⁷³ R. Illingworth,⁴⁶ A.S. Ito,⁴⁶ S. Jabeen,⁷¹
M. Jaffré,¹³ A. Jayasinghe,⁶⁹ M.S. Jeong,²⁸ R. Jesik,⁴¹ P. Jiang,⁴ K. Johns,⁴³ E. Johnson,⁵⁹ M. Johnson,⁴⁶
A. Jonckheere,⁴⁶ P. Jonsson,⁴¹ J. Joshi,⁴⁴ A.W. Jung,⁴⁶ A. Juste,³⁷ E. Kajfasz,¹² D. Karmanov,³⁴ P.A. Kasper,⁴⁶
I. Katsanos,⁶¹ R. Kehoe,⁷³ S. Kermiche,¹² N. Khalatyan,⁴⁶ A. Khanov,⁷⁰ A. Kharchilava,⁶⁴ Y.N. Kharzheev,³²
I. Kiselevich,³³ J.M. Kohli,²⁴ A.V. Kozelov,³⁵ J. Kraus,⁶⁰ A. Kumar,⁶⁴ A. Kupco,⁸ T. Kurča,¹⁷ V.A. Kuzmin,³⁴
S. Lammers,⁵⁰ G. Landsberg,⁷¹ P. Lebrun,¹⁷ H.S. Lee,²⁸ S.W. Lee,⁵³ W.M. Lee,⁴⁶ X. Lei,⁴³ J. Lellouch,¹⁴
D. Li,¹⁴ H. Li,¹¹ L. Li,⁴⁴ Q.Z. Li,⁴⁶ J.K. Lim,²⁸ D. Lincoln,⁴⁶ J. Linnemann,⁵⁹ V.V. Lipaev,³⁵ R. Lipton,⁴⁶
H. Liu,⁷³ Y. Liu,⁴ A. Lobodenko,³⁶ M. Lokajicek,⁸ R. Lopes de Sa,⁶⁶ H.J. Lubatti,⁷⁶ R. Luna-Garcia^{g,29}
A.L. Lyon,⁴⁶ A.K.A. Maciel,¹ R. Madar,¹⁹ R. Magaña-Villalba,²⁹ S. Malik,⁶¹ V.L. Malyshev,³² Y. Maravin,⁵⁵
J. Martínez-Ortega,²⁹ R. McCarthy,⁶⁶ C.L. McGivern,⁴² M.M. Meijer,^{30,31} A. Melnitchouk,⁴⁶ D. Menezes,⁴⁸
P.G. Mercadante,³ M. Merkin,³⁴ A. Meyer,¹⁸ J. Meyer,²⁰ F. Miconi,¹⁶ N.K. Mondal,²⁶ M. Mulhearn,⁷⁵ E. Nagy,¹²
M. Naimuddin,²⁵ M. Narain,⁷¹ R. Nayyar,⁴³ H.A. Neal,⁵⁸ J.P. Negret,⁵ P. Neustroev,³⁶ H.T. Nguyen,⁷⁵
T. Nunnemann,²² J. Orduna,⁷⁴ N. Osman,¹² J. Osta,⁵² M. Padilla,⁴⁴ A. Pal,⁷² N. Parashar,⁵¹ V. Parihar,⁷¹
S.K. Park,²⁸ R. Partridge^{e,71} N. Parua,⁵⁰ A. Patwa,⁶⁷ B. Penning,⁴⁶ M. Perfilov,³⁴ Y. Peters,²⁰ K. Petridis,⁴²
G. Petrillo,⁶⁵ P. Pétroff,¹³ M.-A. Pleier,⁶⁷ P.L.M. Podesta-Lerma^{h,29} V.M. Podstavkov,⁴⁶ A.V. Popov,³⁵
M. Prewitt,⁷⁴ D. Price,⁵⁰ N. Prokopenko,³⁵ J. Qian,⁵⁸ A. Quadt,²⁰ B. Quinn,⁶⁰ M.S. Rangel,¹ K. Ranjan,²⁵
P.N. Ratoff,⁴⁰ I. Razumov,³⁵ P. Renkel,⁷³ I. Ripp-Baudot,¹⁶ F. Rizatdinova,⁷⁰ M. Rominsky,⁴⁶ A. Ross,⁴⁰
C. Royon,¹⁵ P. Rubinov,⁴⁶ R. Ruchti,⁵² G. Sajot,¹¹ P. Salcido,⁴⁸ A. Sánchez-Hernández,²⁹ M.P. Sanders,²²
A.S. Santos^{i,1} G. Savage,⁴⁶ L. Sawyer,⁵⁶ T. Scanlon,⁴¹ R.D. Schamberger,⁶⁶ Y. Scheglov,³⁶ H. Schellman,⁴⁹
C. Schwanenberger,⁴² R. Schwienhorst,⁵⁹ J. Sekaric,⁵⁴ H. Severini,⁶⁹ E. Shabalina,²⁰ V. Shary,¹⁵ S. Shaw,⁵⁹
A.A. Shchukin,³⁵ R.K. Shivpuri,²⁵ V. Simak,⁷ P. Skubic,⁶⁹ P. Slattery,⁶⁵ D. Smirnov,⁵² K.J. Smith,⁶⁴ G.R. Snow,⁶¹
J. Snow,⁶⁸ S. Snyder,⁶⁷ S. Söldner-Rembold,⁴² L. Sonnenschein,¹⁸ K. Soustruznik,⁶ J. Stark,¹¹ D.A. Stoyanova,³⁵
M. Strauss,⁶⁹ L. Suter,⁴² P. Svoisky,⁶⁹ M. Titov,¹⁵ V.V. Tokmenin,³² Y.-T. Tsai,⁶⁵ K. Tschann-Grimm,⁶⁶
D. Tsybychev,⁶⁶ B. Tuchming,¹⁵ C. Tully,⁶³ L. Uvarov,³⁶ S. Uvarov,³⁶ S. Uzunyan,⁴⁸ R. Van Kooten,⁵⁰

W.M. van Leeuwen,³⁰ N. Varelas,⁴⁷ E.W. Varnes,⁴³ I.A. Vasilyev,³⁵ P. Verdier,¹⁷ A.Y. Verkheev,³²
 L.S. Vertogradov,³² M. Verzocchi,⁴⁶ M. Vesterinen,⁴² D. Vilanova,¹⁵ P. Vokac,⁷ H.D. Wahl,⁴⁵ M.H.L.S. Wang,⁴⁶
 J. Warchol,⁵² G. Watts,⁷⁶ M. Wayne,⁵² J. Weichert,²¹ L. Welty-Rieger,⁴⁹ A. White,⁷² D. Wicke,²³
 M.R.J. Williams,⁴⁰ G.W. Wilson,⁵⁴ M. Wobisch,⁵⁶ D.R. Wood,⁵⁷ T.R. Wyatt,⁴² Y. Xie,⁴⁶ R. Yamada,⁴⁶
 S. Yang,⁴ T. Yasuda,⁴⁶ Y.A. Yatsunenko,³² W. Ye,⁶⁶ Z. Ye,⁴⁶ H. Yin,⁴⁶ K. Yip,⁶⁷ S.W. Youn,⁴⁶ J.M. Yu,⁵⁸
 J. Zennamo,⁶⁴ T. Zhao,⁷⁶ T.G. Zhao,⁴² B. Zhou,⁵⁸ J. Zhu,⁵⁸ M. Zielinski,⁶⁵ D. Zieminska,⁵⁰ and L. Zivkovic¹⁴

(The D0 Collaboration*)

¹LAFEX, Centro Brasileiro de Pesquisas Físicas, Rio de Janeiro, Brazil

²Universidade do Estado do Rio de Janeiro, Rio de Janeiro, Brazil

³Universidade Federal do ABC, Santo André, Brazil

⁴University of Science and Technology of China, Hefei, People's Republic of China

⁵Universidad de los Andes, Bogotá, Colombia

⁶Charles University, Faculty of Mathematics and Physics,

Center for Particle Physics, Prague, Czech Republic

⁷Czech Technical University in Prague, Prague, Czech Republic

⁸Center for Particle Physics, Institute of Physics,

Academy of Sciences of the Czech Republic, Prague, Czech Republic

⁹Universidad San Francisco de Quito, Quito, Ecuador

¹⁰LPC, Université Blaise Pascal, CNRS/IN2P3, Clermont, France

¹¹LPSC, Université Joseph Fourier Grenoble 1, CNRS/IN2P3,

Institut National Polytechnique de Grenoble, Grenoble, France

¹²CPPM, Aix-Marseille Université, CNRS/IN2P3, Marseille, France

¹³LAL, Université Paris-Sud, CNRS/IN2P3, Orsay, France

¹⁴LPNHE, Universités Paris VI and VII, CNRS/IN2P3, Paris, France

¹⁵CEA, Irfu, SPP, Saclay, France

¹⁶IPHC, Université de Strasbourg, CNRS/IN2P3, Strasbourg, France

¹⁷IPNL, Université Lyon 1, CNRS/IN2P3, Villeurbanne, France and Université de Lyon, Lyon, France

¹⁸III. Physikalisches Institut A, RWTH Aachen University, Aachen, Germany

¹⁹Physikalisches Institut, Universität Freiburg, Freiburg, Germany

²⁰II. Physikalisches Institut, Georg-August-Universität Göttingen, Göttingen, Germany

²¹Institut für Physik, Universität Mainz, Mainz, Germany

²²Ludwig-Maximilians-Universität München, München, Germany

²³Fachbereich Physik, Bergische Universität Wuppertal, Wuppertal, Germany

²⁴Panjab University, Chandigarh, India

²⁵Delhi University, Delhi, India

²⁶Tata Institute of Fundamental Research, Mumbai, India

²⁷University College Dublin, Dublin, Ireland

²⁸Korea Detector Laboratory, Korea University, Seoul, Korea

²⁹CINVESTAV, Mexico City, Mexico

³⁰Nikhef, Science Park, Amsterdam, the Netherlands

³¹Radboud University Nijmegen, Nijmegen, the Netherlands

³²Joint Institute for Nuclear Research, Dubna, Russia

³³Institute for Theoretical and Experimental Physics, Moscow, Russia

³⁴Moscow State University, Moscow, Russia

³⁵Institute for High Energy Physics, Protvino, Russia

³⁶Petersburg Nuclear Physics Institute, St. Petersburg, Russia

³⁷Institució Catalana de Recerca i Estudis Avançats (ICREA) and Institut de Física d'Altes Energies (IFAE), Barcelona, Spain

³⁸Uppsala University, Uppsala, Sweden

³⁹Taras Shevchenko National University of Kyiv, Kiev, Ukraine

⁴⁰Lancaster University, Lancaster LA1 4YB, United Kingdom

⁴¹Imperial College London, London SW7 2AZ, United Kingdom

⁴²The University of Manchester, Manchester M13 9PL, United Kingdom

⁴³University of Arizona, Tucson, Arizona 85721, USA

⁴⁴University of California Riverside, Riverside, California 92521, USA

⁴⁵Florida State University, Tallahassee, Florida 32306, USA

⁴⁶Fermi National Accelerator Laboratory, Batavia, Illinois 60510, USA

⁴⁷University of Illinois at Chicago, Chicago, Illinois 60607, USA

⁴⁸Northern Illinois University, DeKalb, Illinois 60115, USA

⁴⁹Northwestern University, Evanston, Illinois 60208, USA

⁵⁰Indiana University, Bloomington, Indiana 47405, USA

⁵¹Purdue University Calumet, Hammond, Indiana 46323, USA

⁵²University of Notre Dame, Notre Dame, Indiana 46556, USA

⁵³Iowa State University, Ames, Iowa 50011, USA

⁵⁴University of Kansas, Lawrence, Kansas 66045, USA

⁵⁵Kansas State University, Manhattan, Kansas 66506, USA

⁵⁶Louisiana Tech University, Ruston, Louisiana 71272, USA

⁵⁷Northeastern University, Boston, Massachusetts 02115, USA

⁵⁸University of Michigan, Ann Arbor, Michigan 48109, USA

⁵⁹Michigan State University, East Lansing, Michigan 48824, USA

⁶⁰University of Mississippi, University, Mississippi 38677, USA

⁶¹University of Nebraska, Lincoln, Nebraska 68588, USA

⁶²Rutgers University, Piscataway, New Jersey 08855, USA

⁶³Princeton University, Princeton, New Jersey 08544, USA

⁶⁴State University of New York, Buffalo, New York 14260, USA

⁶⁵University of Rochester, Rochester, New York 14627, USA

⁶⁶State University of New York, Stony Brook, New York 11794, USA

⁶⁷Brookhaven National Laboratory, Upton, New York 11973, USA

⁶⁸Langston University, Langston, Oklahoma 73050, USA

⁶⁹University of Oklahoma, Norman, Oklahoma 73019, USA

⁷⁰Oklahoma State University, Stillwater, Oklahoma 74078, USA

⁷¹Brown University, Providence, Rhode Island 02912, USA

⁷²University of Texas, Arlington, Texas 76019, USA

⁷³Southern Methodist University, Dallas, Texas 75275, USA

⁷⁴Rice University, Houston, Texas 77005, USA

⁷⁵University of Virginia, Charlottesville, Virginia 22904, USA

⁷⁶University of Washington, Seattle, Washington 98195, USA

(Dated: December 24, 2012)

We present measurements of the differential cross section $d\sigma/dp_T^\gamma$ for the associated production of a c -quark jet and an isolated photon with rapidity $|y^\gamma| < 1.0$ and transverse momentum $30 < p_T^\gamma < 300$ GeV. The c -quark jets are required to have $|y^{\text{jet}}| < 1.5$ and $p_T^{\text{jet}} > 15$ GeV. The ratio of differential cross sections for $\gamma + c$ to $\gamma + b$ production as a function of p_T^γ is also presented. The results are based on data corresponding to an integrated luminosity of 8.7 fb^{-1} recorded with the D0 detector at the Fermilab Tevatron $p\bar{p}$ Collider at $\sqrt{s} = 1.96$ TeV. The obtained results are compared to next-to-leading order perturbative QCD calculations using various parton distribution functions, to predictions based on the k_T -factorization approach, and to predictions from the SHERPA and PYTHIA Monte Carlo event generators.

PACS numbers: 13.85.Qk, 12.38.Bx, 12.38.Qk

In hadron-hadron collisions high-energy photons are mainly produced directly in a hard parton scattering process. For this reason, and due to their pointlike electromagnetic coupling to the quarks, they provide a clean probe of parton-level dynamics. Photons in association with a charm (c) quark are produced primarily through the Compton-like scattering process $gc \rightarrow \gamma c$, which dominates up to photon transverse momenta with respect to the beam axis of $p_T^\gamma \approx 70\text{--}80$ GeV, and through quark-antiquark annihilation, $q\bar{q} \rightarrow \gamma g \rightarrow \gamma c\bar{c}$, which dominates at higher p_T^γ [1]. Inclusive $\gamma + c$ production may also originate from processes like $gg \rightarrow c\bar{c}$ or $cg \rightarrow cg$, where the fragmentation of a final state c -quark or gluon produces a photon [1]. Photon isolation requirements substantially reduce the contributions from these processes. Measurements of the $\gamma + c$ -quark jet differential cross section as a function of p_T^γ improve our understanding of the underlying production mechanism and provide useful input for the c -quark parton distribution functions (PDFs) of the colliding hadrons.

In this Letter, we present measurements of the inclusive $\gamma + c$ -jet production cross sections using data col-

lected from June 2006 to September 2011 with the D0 detector in $p\bar{p}$ collisions at $\sqrt{s} = 1.96$ TeV which correspond to an integrated luminosity of $8.7 \pm 0.5 \text{ fb}^{-1}$ [2]. The cross section is measured differentially as a function of p_T^γ for photons within rapidities $|y^\gamma| < 1.0$ and $30 < p_T^\gamma < 300$ GeV, while the c -jet is required to have $|y^{\text{jet}}| < 1.5$ and $p_T^{\text{jet}} > 15$ GeV. In comparison to our previous $\gamma + c$ -jet measurement [3], we now retain all events having at least one jet originating from a charm quark, as opposed to considering only the events in which the charm jet candidate is the jet with highest p_T . To increase the signal yield and study a trend in the data/theory ratio observed in Ref. [3], we have extended the rapidity [4] region from $|y^{\text{jet}}| < 0.8$ to $|y^{\text{jet}}| < 1.5$ and combine regions with positive and negative products of rapidities, $y^\gamma y^{\text{jet}}$. In addition, an increased integrated luminosity by about a factor of nine allows the p_T^γ range to be extended to higher values.

The data set and event selections used in our measurement are similar to those used in the recently published measurement of the $\gamma + b$ -jet differential cross section [5]. However, because of the difficulty in discriminating c jets

*with visitors from ^aAugustana College, Sioux Falls, SD, USA,

^bThe University of Liverpool, Liverpool, UK, ^cUPIITA-IPN, Mexico City, Mexico, ^dDESY, Hamburg, Germany, ^eSLAC, Menlo Park, CA, USA, ^fUniversity College London, London, UK, ^gCentro

from light jets, this measurement adopts a different strategy for the estimation of the c -jet fraction. Here we apply a significantly more stringent requirement for selecting heavy flavor jets (originating from c and b quarks) in order to suppress the rates of light jets (originating from light quarks or gluons) by an additional factor of $2.5 - 3$. This small residual contribution of light jets is then subtracted from the selected data events prior to performing the fit with the discriminant templates of b -jets and c -jets to extract the c -jet fraction. Using this event selection criteria, we reproduce the results for the $\gamma + b$ -jet cross section, measure the $\gamma + c$ -jet cross section and calculate the ratio $\sigma(\gamma + c)/\sigma(\gamma + b)$ in bins of p_T^γ . Common experimental uncertainties and dependence on the higher-order corrections in theory are reduced in the ratio, allowing a precise study of the relative $\sigma(\gamma + c)/\sigma(\gamma + b)$ rates.

The D0 detector is a general purpose detector described in detail elsewhere [6]. The subdetectors most relevant to this analysis are the central tracking system, composed of a silicon microstrip tracker (SMT) and a central fiber tracker (CFT) embedded in a 1.9 T solenoidal magnetic field, the central preshower detector (CPS), and the calorimeter. The CPS is located immediately before the inner layer of the central calorimeter and is formed of approximately one radiation length of lead absorber followed by three layers of scintillating strips. The calorimeter consists of a central section (CC) with coverage in pseudorapidity of $|\eta_{\text{det}}| < 1.1$ [7], and two end calorimeters (EC) extending coverage to $|\eta_{\text{det}}| \approx 4.2$, all housed in separate cryostats, with scintillators between the CC and EC cryostats providing sampling of developing showers for $1.1 < |\eta_{\text{det}}| < 1.4$. The electromagnetic (EM) section of the calorimeter is segmented longitudinally into four layers (EM i , $i = 1 - 4$), with transverse segmentation into cells of size $\Delta\eta_{\text{det}} \times \Delta\phi = 0.1 \times 0.1$ [7], except EM3 (near the EM shower maximum), where it is 0.05×0.05 . The calorimeter allows for a precise measurement of the energy and direction of electrons and photons, providing an energy resolution of approximately 4% (3%) at an energy of 30 (100) GeV, and an angular resolution of about 0.01 radians. The energy response of the calorimeter to photons is calibrated using electrons from Z boson decays. Since electrons and photons interact differently in the detector material before the calorimeter, additional energy corrections as a function of p_T^γ are derived using a detailed GEANT-based [8] simulation of the D0 detector response. These corrections are largest, $\approx 2\%$, at photon energies of about 30 GeV.

The data used in this analysis are collected using a combination of triggers requiring a cluster of energy in the EM calorimeter with loose shower shape requirements. The trigger efficiency is $\approx 96\%$ for photon candidates with $p_T^\gamma \approx 30$ GeV and $\approx 100\%$ for $p_T^\gamma > 40$ GeV.

Offline event selection requires a reconstructed $p\bar{p}$ interaction vertex [9] within 60 cm of the center of the detector along the beam axis. The missing transverse

momentum in the event is required to be less than $0.7p_T^\gamma$ to suppress the background contribution from $W \rightarrow e\nu$ decays. These requirements are highly efficient ($\geq 98\%$) for signal events.

The photon selection criteria in the current measurement are identical to those used in Ref. [5]. The photon selection efficiency and acceptance are calculated using samples of $\gamma + c$ -jet events, generated using the SHERPA [10] and PYTHIA [11] event generators. The samples are processed through a GEANT-based [8] simulation of the D0 detector response, followed by reconstruction using the same algorithms as applied to data. As in Ref. [5], in the efficiency and acceptance calculations the photon is required to be isolated at the particle level by $E_T^{\text{iso}} = E_T^{\text{tot}}(0.4) - E_T^\gamma < 2.5$ GeV, where $E_T^{\text{tot}}(0.4)$ is the total transverse energy of particles within a cone of radius $\mathcal{R} = \sqrt{(\Delta\eta)^2 + (\Delta\phi)^2} = 0.4$ centered on the photon and E_T^γ is the photon transverse energy. The particle level includes all stable particles as defined in Ref. [12]. The photon acceptance varies within (82 – 90)% with a relative systematic uncertainty of (2 – 5)%, while the efficiency to pass photon identification criteria is (68 – 85)% with 3% systematic uncertainty.

At least one jet with $p_T^{\text{jet}} > 15$ GeV and $|y^{\text{jet}}| < 1.5$ must be reconstructed in each event. Jets are reconstructed using the D0 Run II algorithm [13] with a cone radius of $\mathcal{R} = 0.5$. The jet acceptance with respect to the p_T^{jet} and $|y^{\text{jet}}|$ varies between 91% and 100% in different p_T^{jet} bins. Uncertainties on the acceptance due to the jet energy scale, jet energy resolution, and the difference between results obtained with SHERPA and PYTHIA are in the range of (1 – 4)%. A set of criteria is imposed to have sufficient information to classify the jet as a heavy-flavor candidate: the jet is required to have at least two associated tracks with $p_T > 0.5$ GeV with at least one hit in the SMT, and at least one of these tracks must have $p_T > 1.0$ GeV. These criteria have an efficiency of about 90%.

To enrich the sample with heavy-flavor jets, a neural net based b -tagging algorithm (b -NN) is applied. It exploits the longer lifetimes of b -flavored hadrons in comparison to their lighter counterparts, after the rejection of long-lived K_s^0 and Λ decays [14]. The inputs to the b -NN combine information from the impact parameter of displaced tracks and the topological properties of secondary vertices reconstructed in the jet to provide a continuous output value that tends towards one for b jets and zero for light-quark jets. Events are required to contain at least one jet satisfying b -NN output > 0.7 . This b -tagging selection suppresses light jets to less than 5% of the heavy-flavor enhanced sample. The efficiency for b and c jets to satisfy the b -tagging requirements in the simulation is scaled by the data-to-Monte Carlo (MC) correction factors parametrized as a function of jet p_T and η [14]. Depending on p_T^γ , the selection efficiency for this requirement is (8 – 10)% for c -jets with relative

systematic uncertainties of $(6 - 23)\%$, caused by uncertainty on the data-to-MC correction factors. The maximum difference between the efficiencies for c -jets arising from the Compton-like and annihilation subprocesses is about 10%.

The relative rate of remaining light jets (“light/all”) in the sample after the final selection is estimated using SHERPA and PYTHIA γ +jet events, taking into account the data-to-MC correction factors as described in Ref. [14]. The light jet rates predicted by PYTHIA and SHERPA agree within 5%. The central predictions are taken from SHERPA, which agrees with measured γ +jet [15, 16] and γ + b -jet [5] cross sections within $(10 - 25)\%$.

After application of all selection requirements, 130,875 events remain. We estimate the photon purity using an artificial neural network discriminant [5]. The distribution of the output of this discriminant (O_{NN}) is fitted to a linear combination of templates for photons and jets obtained from simulated γ + jet and dijet samples, respectively. An independent fit is performed in each p_T^γ bin. It yields photon purities between 62% and 99%, which are close to those obtained in Ref. [5]. Their systematic uncertainties are of a comparable magnitude, $(5 - 9)\%$.

The invariant mass of all charged particles associated with a displaced secondary vertex in a jet, M_{SV} , is a powerful variable to discriminate c from b jets. Since the M_{SV} templates for light and c -jets after application of tight b -tagging requirements are quite close to each other, we first subtract the remaining small fraction $(1 - 5\%)$ of light jets from the data. Then the c -jet fraction is determined by fitting M_{SV} templates for c and b jets to the $(\gamma$ +heavy flavor jet) data. Jets from b quarks contain secondary vertices that have in general larger values of M_{SV} as compared to c jets and the region beyond $M_{SV} > 2.0$ GeV is strongly dominated by b jets. The templates for b and c jets are obtained from PYTHIA samples of γ + b -jet and γ + c -jet events, respectively, and are consistent with the templates generated using SHERPA. The templates for jets arising from the Compton-like and annihilation subprocesses are also similar to each other.

The result of a maximum likelihood fit to the M_{SV} templates, normalized to the number of events in data, is shown in Fig. 1 for the $50 < p_T^\gamma < 60$ GeV bin as an example. Fits in the other p_T^γ bins are of similar quality. As shown in Fig. 2, the estimated c -jet fraction obtained from the fits in the final selected heavy-flavor sample after subtraction of the light-jet component drops with increasing p_T^γ , on average, from about 52% to about 40%. The corresponding fit uncertainties range between $(4 - 32)\%$, increasing towards higher p_T^γ , and are dominated by the limited data statistics. Since the fits are performed independently in each p_T^γ bin, these uncertainties are uncorrelated from bin to bin. Additional systematic uncertainties are estimated by varying the relative rate of light jets by $\pm 50\%$ and by considering the differences in the light jet predictions from SHERPA and PYTHIA event

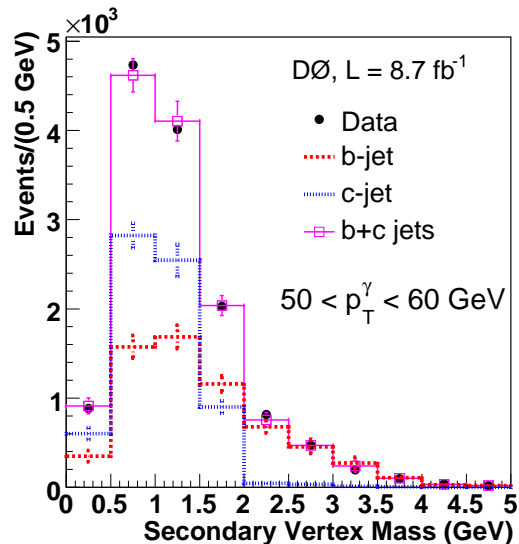


FIG. 1: (Color online) Distribution of secondary vertex mass after all selection criteria for a representative bin of $50 < p_T^\gamma < 60$ GeV. The expected contribution from the light-jet component has been subtracted from the data. The distributions for the b -jet and c -jet templates (with statistical uncertainties) are shown normalized to their respective fitted fractions.

generators. These two sources lead to uncertainties on the c -jet fraction of about $(5 - 9)\%$ and 6% , respectively.

Systematic uncertainty on the measured cross sections due to the b -NN selection is estimated by performing the measurement with looser b -NN selections: requiring b -NN output > 0.3 or > 0.5 instead of 0.7 . In both cases, this significantly increases the light-jet rate and also changes the c - and b -jet fractions, resulting in a variation of the γ + c -jet cross section of $\leq 7\%$. This variation is taken as a systematic uncertainty on the cross section.

The data, corrected for photon and jet acceptance, reconstruction efficiencies and the admixture of background events, are presented at the particle level [12] for comparison with predictions by unfolding the data for effects of detector resolution.

The differential cross sections of γ + c -jet production are extracted in nine bins of p_T^γ . They are listed in Table I and are shown in Fig. 3. The data points are plotted at the values of p_T^γ for which the value of a smooth function describing the dependence of the cross section on p_T^γ equals the averaged cross section in the bin [17].

The statistical uncertainty of the results ranges from 2% in the first p_T^γ bin to 11% in the last p_T^γ bin. The total systematic uncertainty varies between 14% and 42% across these bins. The main sources of uncertainty at low p_T^γ are due to the photon purity (up to 8%), the c -jet fraction $(10 - 33\%)$, and the luminosity (6%) [2]. The total systematic uncertainties (δ_{syst}) and the bin-to-bin uncorrelated components ($\delta_{\text{syst}}^{\text{unc}}$) are shown in Table I.

Next-to-leading order (NLO) perturbative QCD pre-

TABLE I: The $\gamma + c$ -jet production cross sections $d\sigma/dp_T^\gamma$ in bins of p_T^γ for $|y^\gamma| < 1.0$, $p_T^{\text{jet}} > 15$ GeV and $|\eta^{\text{jet}}| < 1.5$ together with statistical uncertainties (δ_{stat}), total systematic uncertainties (δ_{syst}), and the uncorrelated component of δ_{syst} ($\delta_{\text{syst}}^{\text{unc}}$). The column δ_{tot} shows total experimental uncertainty obtained by adding δ_{stat} and δ_{syst} in quadrature. The last four columns show theoretical predictions obtained within NLO QCD, k_T -factorization, and by the PYTHIA and SHERPA event generators.

p_T^γ bin (GeV)	$\langle p_T^\gamma \rangle$ (GeV)	$d\sigma/dp_T^\gamma$ (pb/GeV)								
		Data	δ_{stat} (%)	$\delta_{\text{syst}}(\delta_{\text{syst}}^{\text{unc}})$ (%)	δ_{tot} (%)	NLO QCD	k_T fact.	PYTHIA	SHERPA	
30 – 40	34.2	8.83	2	15 (3)	15	10.5	6.88	6.55	10.0	
40 – 50	44.3	3.02	3	14 (3)	15	2.96	2.19	2.21	3.47	
50 – 60	54.3	1.33	3	14 (4)	14	1.03	8.59×10^{-1}	8.10×10^{-1}	1.36	
60 – 70	64.5	6.15×10^{-1}	3	14 (5)	14	4.15×10^{-1}	4.12×10^{-1}	3.39×10^{-1}	5.52×10^{-1}	
70 – 90	78.1	2.73×10^{-1}	3	14 (5)	14	1.39×10^{-1}	1.68×10^{-1}	1.24×10^{-1}	1.87×10^{-1}	
90 – 110	98.6	8.61×10^{-2}	4	16 (8)	17	3.80×10^{-2}	6.09×10^{-2}	3.90×10^{-2}	5.36×10^{-2}	
110 – 140	122	2.79×10^{-2}	5	19 (11)	19	1.06×10^{-2}	2.34×10^{-2}	1.23×10^{-2}	1.77×10^{-2}	
140 – 180	156	9.54×10^{-3}	7	24 (17)	26	2.49×10^{-3}	7.11×10^{-3}	3.07×10^{-3}	4.39×10^{-3}	
180 – 300	216	1.16×10^{-3}	11	42 (32)	43	2.79×10^{-4}	1.44×10^{-3}	4.01×10^{-4}	5.83×10^{-4}	

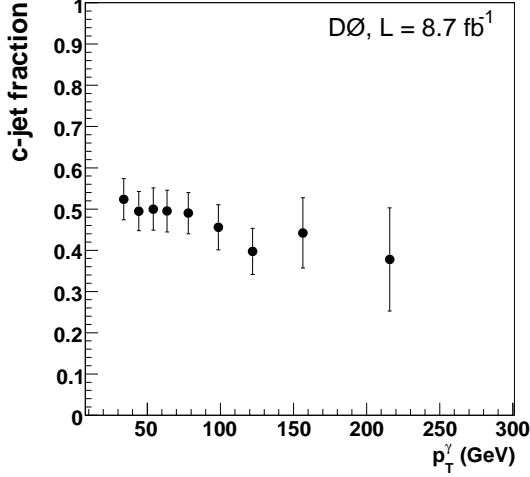


FIG. 2: The c -jet fraction in data after subtraction of light-jet background as a function of p_T^γ derived from the template fit to the heavy quark jet data sample after applying all selections. The error bars include statistical and systematic uncertainties. Binning is the same as given in Table I.

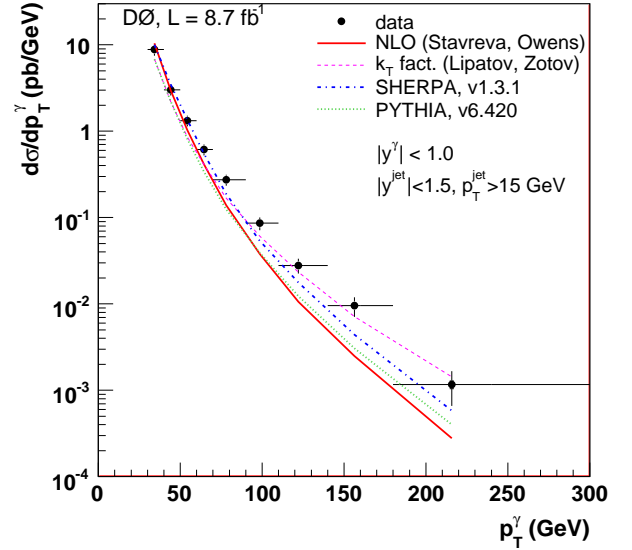


FIG. 3: (Color online) The $\gamma + c$ -jet differential production cross sections as a function of p_T^γ . The uncertainties on the data points include statistical and systematic contributions added in quadrature. The horizontal error bars show the p_T^γ bins. The measurements are compared to the NLO QCD calculations [1, 18] using CTEQ6.6M PDFs [19] (solid line). The predictions from SHERPA [10], PYTHIA [11] and k_T factorization approach [20, 21] are shown by the dash-dotted, dotted and dashed lines, respectively.

dictions of order $\mathcal{O}(\alpha_s^2)$ [1, 18], with the renormalization scale μ_R , factorization scale μ_F , and fragmentation scale μ_f all set to p_T^γ , are given in Table I. The uncertainty from the scale choice is estimated through a simultaneous variation of all three scales by a factor of two, i.e., for $\mu_{R,F,f} = 0.5p_T^\gamma$ and $2p_T^\gamma$, and is found to be similar to those for $\gamma + b$ -jet predictions (5 – 30)%, being larger at higher p_T^γ [5]. The NLO predictions utilize CTEQ6.6M PDFs [19] and are corrected for non-perturbative effects of parton-to-hadron fragmentation and multiple parton interactions. The latter are evaluated using SHERPA and PYTHIA MC samples generated using their default settings [10, 11]. The overall corrections vary within 0.90 – 0.95 with an uncertainty of $\lesssim 2\%$ assigned to account for the difference between the two MC generators.

The predictions based on the k_T -factorization approach [20, 21] and unintegrated parton distributions [22] are also given in Table I. The resummation of gluon diagrams with gluon transverse momentum (k_T) above a scale μ of order 1 GeV, leads to a broadening of the photon transverse momentum distribution in this approach [20]. The scale uncertainties on these predictions vary from about $-28\%/ + 31\%$ at $30 < p_T^\gamma < 40$ GeV to

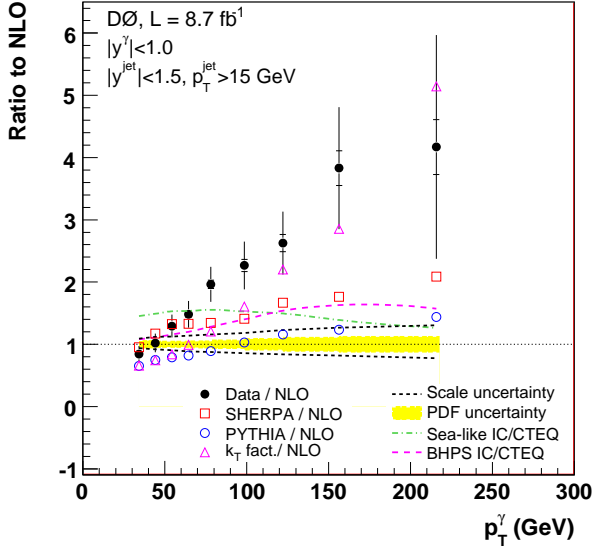


FIG. 4: (Color online) The ratio of $\gamma + c$ -jet production cross sections to NLO predictions for data and theoretical predictions. The uncertainties on the data include both statistical (inner error bar) and total uncertainties (full error bar). Also shown are the uncertainties on the theoretical QCD scales and the CTEQ6.6M PDFs. The ratio for intrinsic charm models [26] are presented, as well as the predictions given by k_T -factorization [20, 21], SHERPA [10] and PYTHIA [11].

about $+14\%/+5\%$ in the last p_T^γ bin.

Table I also contains predictions from the PYTHIA [11] event generator with the CTEQ6.1L PDF set. It includes only $2 \rightarrow 2$ matrix elements (ME) with $gc \rightarrow \gamma c$ and $q\bar{q} \rightarrow \gamma g$ scatterings (defined at LO) followed by $g \rightarrow c\bar{c}$ splitting in the parton shower (PS). We also provide predictions by the SHERPA MC event generator [10] with the CTEQ6.6M PDF set [19]. Matching between the ME partons and the PS jets follows the prescription given in Ref. [15], with the matching scale taken to be 15 GeV. Systematic uncertainties are estimated by varying the ME-PS matching scale by ± 5 GeV around the chosen central value [23], resulting in a $\pm 7\%$ cross section variation.

All theoretical predictions are obtained using the photon isolation requirement of $E_T^{\text{iso}} < 2.5$ GeV. The predictions are compared to data in Fig. 3 as a function of p_T^γ . The ratios of data over the NLO QCD calculations and of the various theoretical predictions to the NLO QCD calculations are presented in Fig. 4. The NLO predictions with CTEQ6.6M agree with MSTW2008 [24] and ABKM09NLO [25] within 10%. Parameterizations for models containing intrinsic charm (IC) have been included in CTEQ6.6c [26]. Here we consider the BHPS IC model [27, 28], based on the Fock space picture of the nucleon structure [29], in which intrinsic charm appears

mainly at large momentum fractions x , and the sea-like model in which the charm PDF is sea-like, similar to that of the light-flavor sea quarks. The NLO QCD predictions based on these intrinsic charm models are normalized to the standard CTEQ predictions and are also shown in Fig. 4. Both non-perturbative intrinsic charm models predict a higher $\gamma + c$ -jet cross section. In the case of the BHPS model, the ratio grows with p_T^γ , while an opposite trend is exhibited by the sea-like model.

The measured cross sections are in agreement with the NLO QCD predictions within theoretical and experimental uncertainties in the region of $30 < p_T^\gamma \lesssim 70$ GeV, but show systematic disagreement for larger p_T^γ . The cross section slope in data differs significantly from the NLO QCD prediction. The results suggest a need for higher-order perturbative QCD corrections in the large p_T^γ region, which is dominated by the annihilation process $q\bar{q} \rightarrow \gamma g$ (with $g \rightarrow c\bar{c}$), and resummation of diagrams with additional gluon radiation. In addition, the underestimation of the rates for diagrams with $g \rightarrow c\bar{c}$ splittings may result in lower theoretical predictions of cross sections as suggested by LEP [30], LHCb [31] and ATLAS [32] results. The prediction from the k_T -factorization approach is in better agreement with data at $p_T^\gamma > 120$ GeV. However, it underestimates the cross section in the low and intermediate p_T^γ region. The $\gamma + c$ -jet cross section as predicted by SHERPA becomes higher than the NLO QCD prediction at large p_T^γ , but is still lower than the measured values. It has been suggested that combining NLO parton-level calculations for the ME with PS predictions [33] will improve the description of the data [34].

In addition to measuring the $\gamma + c$ -jet cross-section, we also obtain results for the $\gamma + b$ -jet cross section using the new tight b -NN selection. The values of the obtained $\gamma + b$ -jet cross section agree within 10% (i.e. within uncertainties) with the published results [5] obtained with a looser b -NN selection. We use them to calculate the ratio $\sigma(\gamma + c)/\sigma(\gamma + b)$ in bins of p_T^γ . In this ratio, many experimental systematic uncertainties cancel. Also, theory predictions of the ratio are less sensitive to the scale uncertainties, and effects from missing higher-order terms that impact the normalizations of the cross sections. The remaining uncertainties are caused by largely (65 – 67%) correlated uncertainties coming from the fitting of c -jet and b -jet M_{SV} templates to data, and by other uncertainties on the c -jet fractions discussed above. The systematic uncertainties on the ratio vary within (6 – 26)%, being largest at high p_T^γ . Theoretical scale uncertainties, estimated by varying scales by a factor of two (to $\mu_{R,F,f} = 0.5p_T^\gamma$ and $2p_T^\gamma$) in the same way for $\sigma(\gamma + c)$ and $\sigma(\gamma + b)$ predictions, are also significantly reduced. Specifically, residual scale uncertainties are typically $\lesssim 10\%$ for the k_T -factorization approach and $\lesssim 4\%$ for NLO QCD, which indicates a much smaller dependence of the ratio on the higher-order corrections.

TABLE II: The $\sigma(\gamma + c)/\sigma(\gamma + b)$ cross section ratio in bins of p_T^γ for $|y^\gamma| < 1.0$, $p_T^{\text{jet}} > 15$ GeV and $|\eta^{\text{jet}}| < 1.5$ together with statistical uncertainties (δ_{stat}), total systematic uncertainties (δ_{syst}), and the uncorrelated component of δ_{syst} ($\delta_{\text{syst}}^{\text{unc}}$). The column δ_{tot} shows total experimental uncertainty obtained by adding δ_{stat} and δ_{syst} in quadrature. The last four columns show theoretical predictions obtained using NLO QCD, k_T -factorization, PYTHIA and SHERPA event generators.

p_T^γ bin (GeV)	$\langle p_T^\gamma \rangle$ (GeV)	$\sigma(\gamma + c)/\sigma(\gamma + b)$							
		Data	δ_{stat} (%)	$\delta_{\text{syst}}(\delta_{\text{syst}}^{\text{unc}})$ (%)	δ_{tot} (%)	NLO QCD	k_T fact.	PYTHIA	SHERPA
30 – 40	34.2	5.83	1	6 (3)	6	5.81	4.30	5.10	6.17
40 – 50	44.3	5.03	1	6 (3)	6	5.28	4.01	4.97	5.28
50 – 60	54.3	4.90	1	7 (3)	7	4.79	3.83	4.66	4.79
60 – 70	64.5	4.55	1	8 (4)	8	4.37	3.91	4.34	4.21
70 – 90	78.1	4.97	1	8 (4)	8	3.83	3.88	3.99	3.54
90 – 110	98.6	4.22	2	9 (6)	9	3.19	3.83	3.59	2.95
110 – 140	122	3.73	3	10 (6)	11	2.60	3.86	3.00	2.50
140 – 180	156	4.34	5	13 (10)	14	2.12	3.53	2.44	2.19
180 – 300	216	3.38	8	26 (22)	27	1.73	4.04	1.98	1.93

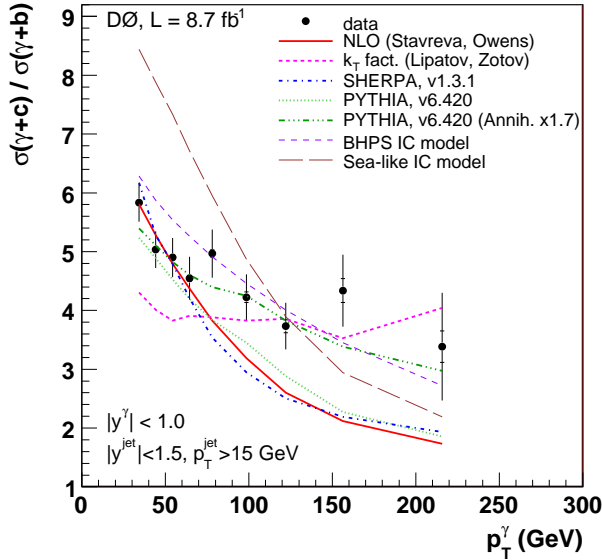


FIG. 5: (Color online) The ratio of $\gamma + c$ -jet and $\gamma + b$ -jet production cross sections for data together with theoretical predictions as a function of p_T^γ . The uncertainties on the data include both statistical (inner error bar) and total uncertainties (full error bar). Predictions given by k_T -factorization [20, 21], SHERPA [10] and PYTHIA [11] are also shown. The PYTHIA predictions with a contribution from the annihilation process increased by a factor of 1.7 are shown as well. The predictions for intrinsic charm models [26] are also presented.

Experimental results as well as theoretical predictions for the ratios are presented in Table II.

Figure 5 shows the measured ratio $\sigma(\gamma + c)/\sigma(\gamma + b)$ as a function of p_T^γ and a comparison with various predictions. There is good agreement with NLO QCD, SHERPA and PYTHIA predictions in the region $30 < p_T^\gamma \lesssim 70$ GeV, while k_T -factorization predicts smaller ratios than observed in data. At higher p_T^γ , data show systematic-

cally higher ratios than NLO QCD, SHERPA and PYTHIA predictions, while k_T -factorization starts agreeing with data within uncertainties. We also show NLO predictions with the BHPS [27, 28] and sea-like IC models [26] used to predict $\gamma + c$ -jet cross section, while standard CTEQ6.6M is used to predict the $\gamma + b$ -jet cross section. The BHPS model agrees with data at $p_T^\gamma > 80$ GeV, while the sea-like model is significantly beyond the range of data points. BHPS model would better describe the ratio to data with a small shift in normalization. As with the $\gamma + c$ -jet measurement, the $\sigma(\gamma + c)/\sigma(\gamma + b)$ ratio can also be better described by larger $g \rightarrow c\bar{c}$ rates than those used in the current NLO QCD, SHERPA and PYTHIA predictions. To test this, we have increased the rate of the annihilation process (where c jet is always produced due to $g \rightarrow c\bar{c}$ splitting) in the PYTHIA predictions. The best description of data is achieved by increasing the rates by a factor of 1.7 with $\chi^2/\text{ndf} \simeq 0.7$ (compared to $\chi^2/\text{ndf} = 4.1$ if such a factor is unity). However, according to our estimates using the signal events simulated with SHERPA, there are also about (10–35)% (higher for larger p_T^γ) events with two c -jets. Assuming that one jet is coming from gluon initial state radiation followed by $g \rightarrow c\bar{c}$ splitting, the required overall correction factor would be smaller by about (8–24)%.

In conclusion, we have measured the differential cross section of $\gamma + c$ -jet production as a function of p_T^γ at the Fermilab Tevatron $p\bar{p}$ collider. Our results cover the kinematic range $30 < p_T^\gamma < 300$ GeV, $p_T^{\text{jet}} > 15$ GeV, $|y^\gamma| < 1.0$, and $|y^{\text{jet}}| < 1.5$. In the same kinematic region, and in the same p_T^γ bins, we have measured the $\sigma(\gamma + c)/\sigma(\gamma + b)$ cross section ratio. None of the theoretical predictions considered give good description of the data in all p_T^γ bins. Such a description might be achieved by including higher-order corrections into the QCD predictions, while at $p_T^\gamma \gtrsim 80$ GeV the observed difference from data may also be caused by an underestimated contribution from gluon splitting $g \rightarrow c\bar{c}$ [30–32] in the annihilation process or by contribution from intrinsic charm.

The presented results can be used for further development of theoretical models to understand production of high energy photons in association with heavy flavor jets.

We are grateful to the authors of the theoretical calculations, T. Stavreva, J. Owens, N. Zotov, and F. Siegert for providing dedicated predictions and for many useful discussions.

We thank the staffs at Fermilab and collaborating institutions, and acknowledge support from the DOE and NSF (USA); CEA and CNRS/IN2P3 (France); MON, NRC KI and RFBR (Russia); CNPq, FAPERJ, FAPESP and FUNDUNESP (Brazil); DAE and DST (India); Colciencias (Colombia); CONACyT (Mexico); NRF (Korea); FOM (The Netherlands); STFC and the Royal Society (United Kingdom); MSMT and GACR (Czech Republic); BMBF and DFG (Germany); SFI (Ireland); The Swedish Research Council (Sweden); and CAS and CNSF (China).

-
-
- [1] T. Stavreva, J.F. Owens, Phys. Rev. D **79**, 054017 (2009).
 - [2] T. Andeen *et al.*, FERMILAB-TM-2365 (2007).
 - [3] V.M. Abazov *et al.* (D0 Collaboration), Phys. Rev. Lett. **102**, 192002 (2009).
 - [4] The rapidity y is related to the polar scattering angle θ with respect to the proton beam axis by $y = 0.5 \ln[(1 + \beta \cos \theta)/(1 - \beta \cos \theta)]$, where β is defined as the ratio between momentum and energy $\beta = |\vec{p}|/E$.
 - [5] V.M. Abazov *et al.* (D0 Collaboration), Phys. Lett. B **714**, 32 (2012).
 - [6] V.M. Abazov *et al.* (D0 Collaboration), Nucl. Instrum. Methods in Phys. Res. A **565**, 463 (2006); R. Angstadt *et al.*, Nucl. Instrum. Methods Phys. Res. A **622**, 298 (2010). M. Abolins *et al.*, Nucl. Instrum. Methods in Phys. Res. A **584**, 75 (2008).
 - [7] The polar angle θ and the azimuthal angle ϕ are defined with respect to the positive z axis, which is along the proton beam direction. Pseudorapidity is defined as $\eta = -\ln[\tan(\theta/2)]$. Also, η_{det} is the pseudorapidity measured with respect to the center of the detector.
 - [8] R. Brun, F. Carminati, CERN Program Library Long Writeup, W5013, (1993); we use GEANT version v3.21.

- [9] The primary $p\bar{p}$ interaction vertex is the most likely hard collision point, among possibly several collisions within a specific beam crossing. The algorithm for defining primary vertex can be found in [14].
- [10] T. Gleisberg *et al.*, J. High Energy Phys. **02**, 007 (2009). We use SHERPA version v1.3.1.
- [11] T. Sjöstrand, S. Mrenna, P.Z. Skands, J. High Energy Phys. **05**, 026 (2006). We use PYTHIA version v6.420 with tune A.
- [12] C. Buttar *et al.*, arXiv:0803.0678 [hep-ph], Section 9.
- [13] G.C. Blazey *et al.*, arXiv:hep-ex/0005012 (2000).
- [14] V.M. Abazov *et al.* (D0 Collaboration), Nucl. Instrum. Methods in Phys. Res. A **620**, 490 (2010).
- [15] S. Höche, S. Schumann, F. Siegert, Phys. Rev. D **81**, 034026 (2010).
- [16] V.M. Abazov *et al.* (D0 Collaboration), paper in preparation.
- [17] G.D. Lafferty, T.R. Wyatt, Nucl. Instrum. Methods in Phys. Res. A **355**, 541 (1995).
- [18] B.W. Harris, J. Owens, Phys. Rev. D **65**, 094032 (2002).
- [19] W.K. Tung *et al.*, J. High Energy Phys. **02**, 052 (2007).
- [20] A.V. Lipatov, N.P. Zotov, J. Phys. G **34**, 219 (2007); S.P. Baranov, A.V. Lipatov, N.P. Zotov, Eur. Phys. J. C **56**, 371 (2008).
- [21] A.V. Lipatov, M.A. Malyshev, N.P. Zotov, J. High Energy Phys. **05**, 104 (2012).
- [22] M.A. Kimber, A.D. Martin, M.G. Ryskin, Phys. Rev. D **63**, 114027 (2001).
- [23] We choose the following ME-PS matching parameters: the energy scale $Q_0 = 15$ GeV and parameter $D = 0.4$, where D is taken to be of the size of the photon isolation cone.
- [24] A. D. Martin, W. J. Stirling, R. S. Thorne, G. Watt, Eur. Phys. J. C **63**, 189 (2009).
- [25] S. Alekhin *et al.*, Phys. Rev. D **81**, 014032 (2010).
- [26] J. Pumplin *et al.*, Phys. Rev. D **75**, 054029 (2007).
- [27] S.J. Brodsky, P. Hoyer, C. Peterson, N. Sakai, Phys. Lett. B **93**, 451 (1980).
- [28] Wen-Chen Chang and Jen-Chieh Peng, Phys. Rev. Lett. **106**, 252002 (2011).
- [29] S.J. Brodsky, SLAC-PUB-10871 [hep-ph/0412101]; S.J. Brodsky, Few Body Syst. **36**, 35 (2005).
- [30] C. Amsler, Phys. Lett. B **667**, 1 (2008); see Section 17.8.
- [31] R. Aaij *et al.* (LHCb Collaboration), J. High Energy Phys. **06**, 141 (2012).
- [32] G. Aad *et al.* (ATLAS Collaboration), Phys. Rev. D **85**, 052005 (2012).
- [33] S. Höche, F. Krauss, M. Schönherr, F. Siegert, arXiv:1207.5030 [hep-ph].
- [34] M. Schönherr, private communications.